

Received 17 December 2022, accepted 11 January 2023, date of publication 16 January 2023, date of current version 20 January 2023.

Digital Object Identifier 10.1109/ACCESS.2023.3236966

## RESEARCH ARTICLE

# M-Ary QAM Asynchronous-NOMA D2D Network With Cyclic Triangular-SIC Decoding Scheme

VISHAKA BASNAYAKE<sup>1,2</sup>, DUSHANTHA NALIN K. JAYAKODY<sup>3</sup>, (Senior Member, IEEE),  
HAKIM MABED<sup>2</sup>, AMBRISH KUMAR<sup>1</sup>,  
AND THARINDU D. PONNIMBADUGE PERERA<sup>1</sup>, (Member, IEEE)

<sup>1</sup>Centre for Telecommunication Research, School of Engineering, Sri Lanka Technological Campus, Padukka 10500, Sri Lanka

<sup>2</sup>DISC/FEMTO-ST, University Bourgogne Franche-Comté, 25200 Montbéliard, France

<sup>3</sup>Centro de Investigaçã em Tecnologias, Autónoma TechLab, Universidade Autónoma de Lisboa, 1169-023 Lisbon, Portugal

Corresponding author: Dushantha Nalin K. Jayakody (nalin.jayakody@ieee.org)

This research was funded by the Fundação para a Ciência e a Tecnologia, Portugal under Grant No.:2022.03897.PTDC and CEU-Cooperativa de Ensino Universitário, Portugal.

**ABSTRACT** The complexity of successive interference cancellation at the receiver's end is a challenging issue in conventional non-orthogonal multiple access assisted massive wireless networks. The computational complexity of decoding increases exponentially with the number of users. Further, under realistic channel conditions, a synchronous non-orthogonal multiple access scheme is impractical in the uplink device-to-device communications. In this paper, an asynchronous non-orthogonal multiple access-based cyclic triangular successive interference cancellation scheme is proposed for a massive device-to-device network. The proposed scheme reduces the decoding complexity, energy consumption, and bit error rate of a superimposed signal received in an outband device-to-device network. More specifically, the scheme follows three consecutive stages; optimization, decoding, and re-transmission. In the optimization stage, a dual Lagrangian objective function is defined to maximize the number of data symbols decoded at the receiver by determining an optimal interference cancellation triangle, under the co-channel interference and data rate constraints. In the decoding stage, the data in the optimal interference cancellation triangle is decoded using a conventional triangular successive interference cancellation technique. Next, the remaining users' data are decoded in sequential iterations of the proposed scheme, using the retransmissions from such users. Utilizing the successive interference cancellation characteristics, the performance of the proposed device-to-device network is defined in terms of energy efficiency, bit error rate, computational complexity, and decoding delay metrics. Moreover, the performance of the proposed decoding scheme is compared with the conventional triangular successive interference cancellation decoding scheme to demonstrate the superiority of the proposed scheme.

**INDEX TERMS** Asynchronous non-orthogonal multiple access, cyclic triangular successive interference cancellation, device-to-device communication network, decoding complexity, energy consumption, optimization, reliability.

## I. INTRODUCTION

The forthcoming beyond-5G/6G network is expected to provide reliable, error-free, and energy-efficient services with ubiquitous connectivity [1], [2], [3]. On the other hand, the usage of new wireless devices is also increasing mobile traffic

The associate editor coordinating the review of this manuscript and approving it for publication was Xiaofan He.

by thousand times in comparison to the existing networking systems [4]. In this context, widely used 5G Orthogonal Multiple Access (OMA) schemes such as Orthogonal Frequency Division Multiple Access (OFDMA) [5] and Code Division Multiple Access (CDMA) [6] can support a large number of devices by utilizing the existing network resources effectively. Moreover, in OFDMA, the complete bandwidth of the channel is allocated to all the sub-carriers in such a

manner that the interference between each sub-carriers can be minimized. Since the number of sub-carriers within the bandwidth is limited, OFDMA suffers from spectrum limitation issues in public networks.

Non-Orthogonal Multiple Access (NOMA) scheme is included in 3GPP as a multiple access scheme for 5G/6G [7]. This has the potential to enhance the spectral efficiency, by allowing multiple users to simultaneously access the same subcarrier Resource Blocks (RBs) [8]. The fundamental concept of NOMA is based on superposition coding and successive decoding where the superposition coding of multiple users' signals can be done over the same subcarrier with different power levels that enables the receiver to decode the signal by using the Successive Interference Cancellation (SIC) technique [9], [10]. At the receiver, the SIC treatment is applied to decode the data of the user having the strongest channel conditions up to the last user in descending order of Signal to Noise Ratios (SNRs). Once the strongest signal is directly decoded, the detected data is passed through to an iterative SIC algorithm. Next, the strongest signal is reconstructed based on the prior knowledge of Channel State Information (CSI) and the modulation scheme used for transmission. Finally, the reconstructed signal is subtracted from the received superimposed symbol to reduce its interference and increase accuracy in decoding the rest of the user signals. However, the SIC decoding scheme is applicable only for time-synchronous transmissions that limits the NOMA scheme performance, due to the negligence of the added interference from the overlapping symbols [7], [8], [9], [10], [11], [12], [13], [14].

In D2D networks, the users are geographically distributed and their respective signals propagate over different paths that encounter distinct channel effects [15]. As a consequence, all signals arrive at the receiving terminal with varying time offsets and hence, time-synchronous data reception is not possible at the receiver terminal of a D2D network [16]. In [17], an Asynchronous NOMA (A-NOMA) scheme has been proposed under the consideration that the interference is induced by co-channel during the decoding process of the desired user's data symbols at the receiver terminal. Therefore, the studies in [11], [17], [18], [19], and [20] have illustrated that the use of the A-NOMA scheme can improve the decoding ability of the receiver terminal as well as enhance the D2D network performance. Such studies claim that the asynchrony between user signals can in-fact enhance spectral efficiency. In [21], it has been proven that the asynchrony in the transmission can enhance the signal detection at the receiver terminal in an uplink A-NOMA scheme even under equal-power asynchronous transmissions. Moreover, in [22], it has been defined that the optimal mismatch between user signals in an uplink A-NOMA can enhance the throughput and energy efficiency. Authors in [18] have proposed and experimentally implemented an A-NOMA scheme for an uplink optical access scenario, which has a higher Bit Error Rate (BER) reduction of one order magnitude than the synchronous NOMA schemes. Moreover, in [19], an uplink

A-NOMA with a sufficiently large data frame length has been shown to outperform synchronous NOMA in terms of sum throughput.

Other than spectral efficiency and reliability metrics, one of the main targets of future 6G D2D networks is to optimize its' Energy Efficiency (EE) [1], [3], [23], [24], [25]. Nowadays, massive Device-to-Device (D2D) networks are in demand due to their key merits namely i) infrastructure-free network, ii) ability to operate with limited resources and iii) ubiquitous connectivity to the end-users. Indeed, a massive NOMA-assisted D2D network conventionally suffers from high complexity during the decoding phase [26], [27]. Moreover, the authors in [28] have shown that there is an increase in decoding complexity in the NOMA scheme when the number of users increases for more than three. Thus, an increment incur high complexity that reduce the energy efficiency of the D2D networks. The energy consumption at mobile devices can be higher, particularly in energy limited D2D communication scenarios such as emergency disaster scenarios, since such devices cannot cope flexibly with energy consuming computations [2], [29]. Additionally, limited resources for allocation, complex SIC decoding procedure can be observed in NOMA based massive D2D networks. Hence, it was noted that, a reliable and an efficient A-NOMA for massive D2D networks is understudied.

Recently, in [17], an iterative signal processing based Triangular-SIC (T-SIC) technique has been proposed to enhance the spectral efficiency of A-NOMA uplink transmissions. Due to the triangular pattern used for decoding symbols in T-SIC, the interference caused by multiple asynchronous data symbols on each desired user's symbols is considered to enhance the symbol detection and residual interference cancellation in D2D network. Therefore, the T-SIC technique can also be exploited to optimize the decoding ability and spectrum efficiency of the A-NOMA D2D network. To the best of authors' knowledge, it is yet not been used in D2D networks to date. The overall objective of this paper is to investigate and optimize the performance of massive A-NOMA D2D transmissions under a modulation such as *M*-ary QAM. The fourfold contributions of this work are summarized as follows:

- A novel binary optimization algorithm is proposed to decide the optimal combination of data symbols in the received superimposed signal to be decoded under maximum co-channel interference and minimum data rate constraints. The corresponding optimization problem is a hard constraint problem due to its binary optimization variables and non-linear constraints. Hence, such binary variables and non-linear constraints are reformulated to form continuous and linear constraints, and a Lagrangian dual objective function is formed. Then, this can be solved efficiently by applying the Lagrangian dual algorithm.
- Moreover, a new Cyclic T-SIC scheme is proposed to ensure the decoding of each user's data in consecutive iterations, considering also the retransmissions by the

users whose data were not yet decoded in a prior iteration of optimization. Moreover, the EE and BER performance of the Cyclic T-SIC is shown to be significant in comparison to Conventional T-SIC (Conv T-SIC).

- The optimal trade-off between the BER and EE of the proposed Cyclic T-SIC is studied, and compared with conventional Conv T-SIC. The Cyclic T-SIC achieves a higher EE and reduced BER with a lower transmit SNR, lower received power ratio, and higher asynchrony among user signals as compared to a competitive scheme, Conv T-SIC.
- The computational complexity of the proposed Cyclic T-SIC over  $n$  iterations is less than that of the Conv T-SIC scheme when the error tolerance for algorithm termination,  $\epsilon$ , is in the order of  $10^{-1}$  magnitude. Further, the total simulation delay is shown to be lesser in Cyclic T-SIC than Conv T-SIC due to its reduced computational complexity.

The remaining of this paper is organized as follows. In Section II, the existing A-NOMA T-SIC scheme is introduced, and in the Section III the received signal structure and the iterative signal processing at the receiver are presented. Section III-A presents the problem formulation and the proposed Cyclic T-SIC scheme is presented in Section III-B. Next, the performance analysis is given in Section IV. Furthermore, a numerical result analysis is presented in Section V. Finally, conclusions are drawn with remarks in Section VI.

## II. SYSTEM MODEL

In this section, a D2D A-NOMA signal model and its preliminaries are presented. Hence, an A-NOMA assisted D2D network with  $k \in K$  geographically distributed transmitting users, where  $K$  is the maximum number of transmitters, and one receiving terminal,  $R_X$ , within a small neighborhood is considered as shown in Figure 1. It is assumed that there are  $K$  NOMA users sharing each subcarrier with  $N$  subcarriers, and  $K \geq 1$ . It is assumed that the transmitted signals are not aligned at the receiver, and hence the channel is symbol asynchronous. Therefore, a power domain A-NOMA scheme-assisted decoding method is applied in our proposed work where the waveform technique used is based on Orthogonal Frequency Division Multiplexing (OFDM) [12], [16], [17], [19], [30], [31].

Moreover, due to the timing offset between users in A-NOMA, inter-carrier interference (ICI) can occur and the resultant OFDM frequency components can get distorted. Such ICI at a subcarrier is formulated as follows. Consider an OFDM signal at time  $t$  modeled as:

$$x(t) = \sum_{n=1}^N X[n]e^{jw\pi f_n t}, \quad (1)$$

where  $f_n$  is the frequency of the  $n^{th}$  subcarrier,  $0 \leq t \leq T_N$  and  $j$  denotes the complex number. Moreover,  $T_N$  is the symbol time, and  $X[n]$  is the signal transmitted over the  $n$ th subcarrier. Furthermore, the frequency offset due to asynchrony

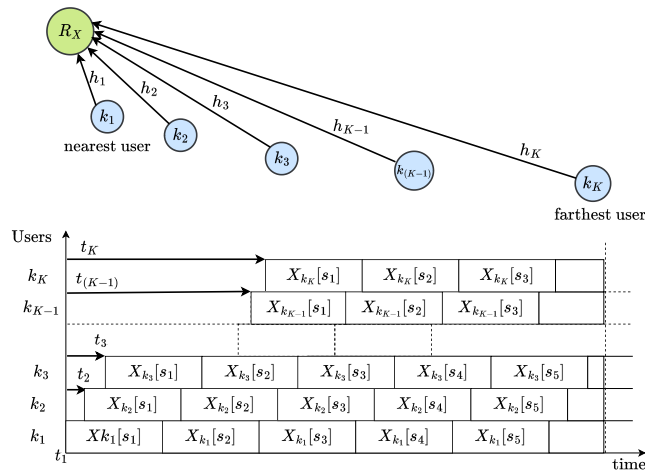


FIGURE 1. A-NOMA assisted D2D communication with a  $K$  number of transmitters and one receiving UE.

in the A-NOMA signal will introduce a multiplicative time-varying distortion, represented as  $\beta(t) = e^{j2\pi\rho\Delta ft}$ , where  $\rho = \frac{\delta f}{\Delta f}$ . As a result, the ICI on the  $m^{th}$  subcarrier is modeled as [17]:

$$ICI_m = \sum_{n=1, n \neq m}^N \int_0^{T_N} X[n]e^{j2\pi\rho\Delta ft} e^{-j2\pi\Lambda\Delta ft} dt, \quad (2)$$

where the  $\Lambda$  gives the distance of the interfering subcarrier to the desired subcarrier. Meanwhile, in NOMA systems Multi-Access Interference (MAI) given in (4) is another interference that can distort the OFDM symbol of the desired user. Also, it is noted that in A-NOMA, the ICI is comparatively lesser than Multi-Access Interference [17]. Hence, for this analysis, the MAI is considered the dominant source of interference, and one subcarrier is focused on for the analysis.

The received signal at  $R_X$  for the  $k^{th}$  user at the  $s$ th symbol is given by [17],

$$Y_{k^*}[s] = h_{k^*} \cdot \sqrt{P_{k^*}} \cdot X_{k^*}[s] + \eta_{k^*}[s] + n_0, \quad (3)$$

where  $X_{k^*}[s]$  denotes the  $k^*$ th user's  $s$ th data symbol which is complex and output from a M-ary-QAM symbol mapper, and  $P_{k^*}$  is the transmit power of  $X_{k^*}[s]$ , which is same for all symbols of  $k^*$ th user for transmission time duration. Hence, the signal transmitted from the  $k^*$ th user at the  $s$ th symbol can be denoted by  $\sqrt{P_{k^*}}X_{k^*}[s]$ . The frequency response on one subcarrier for one symbol time period is considered flat and assumed to follow a Rayleigh distribution independently and identically (i.i.d) [32], [33], [34]. The symbol time is assumed to be considerably lesser than the channel coherence time. Hence,  $h_{k^*}[s]$  is constant for a block of symbols during a transmission period. Further,  $n_0$  is the Additive White Gaussian Noise (AWGN) at the receiver side with variance  $\sigma^2$  and  $\eta_{k^*}[s]$  is the total interference to the

<sup>1</sup> $k^*$  indicates the desired user within a cohort of  $K$  users.

$k^*$ th user's  $s$ th symbol [17].

$$\eta_{k^*}[s] = \sum_{i \neq k^*}^K \sum_{\zeta=s-1}^{s+1} \Delta_{k^*,i}[s, \zeta]. X_i[\zeta]. h_i. \sqrt{P_i}. e^{j\theta_{k^*,i}}, \quad (4)$$

where  $e^{j\theta_{k^*,i}}$  depicts the  $i^{\text{th}}$  user's phase mismatch of the signal to the  $k^*$ th and  $\Delta_{k^*,i}$  denotes the symbol duration that the  $i^{\text{th}}$  user's  $\zeta$  symbol overlap with the desired symbol, as a percentage out of the total symbol period,  $T_{\text{sym}}$ . Moreover, research works such as [35], [36], and [37] have addressed the problem of estimating the time offset, and carrier offset which leads to estimating  $\Delta_{k^*,i}$  and  $\theta_{k^*,i}$  with high reliability in D2D communications using time of arrival measurements.

Following the standard SIC procedure, after subtracting the reconstructed interference,  $\hat{\eta}_{k^*,i}[s, \zeta]$ , of all overlapping interferer's symbols, the remaining interference cancelled signal for desired symbol is formulated in terms of desired signal, residual interference plus noise as [17],

$$\begin{aligned} \tilde{Y}_{k^*}[s] &= Y_{k^*}[s] - \sum_{i \neq k^*}^K \sum_{\zeta=s-1}^{s+1} \hat{\eta}_{k^*,i}[s, \zeta], \\ &= X_{k^*}[s]. h_{k^*} \sqrt{P_{k^*}} + \tilde{\eta}_{k^*}[s] + n_0, \end{aligned} \quad (5)$$

where the latest residual interference to the desired symbol,  $k^*[s]$ , is modelled as [17],

$$\tilde{\eta}_{k^*}[s] = \sum_{i \neq k^*}^K \sum_{\zeta=s-1}^{s+1} \Delta_{k^*,i}[s, \zeta]. (X_i[\zeta] - \hat{X}_i[\zeta]). h_i \sqrt{P_i}. e^{j\theta_{k^*,i}}. \quad (6)$$

Moreover, such residual interference is utilized in the A-NOMA T-SIC scheme to improve the decoding reliability.

### III. PROBLEM FORMULATION

First, the Conventional T-SIC (Conv T-SIC) scheme [17] that can enhance the decoding performance in A-NOMA uplink transmissions is presented. Secondly, a new Cyclic T-SIC scheme that can be applied in A-NOMA D2D networks is proposed.

#### A. CONV T-SIC DECODING SCHEME

The Conv T-SIC decoding scheme [17] is applicable at the receiver  $R_X$  terminal for a communication system containing  $k \in K$  transmitters as shown in Figure 1. The T-SIC decoding procedure is followed once an asynchronous superimposed signal with misaligned data symbols is received at  $R_X$ . First an Interference Cancellation (IC) triangle is constructed by exploiting the triangular pattern of data symbols detected. The weakest symbol received out of such data symbols is added to the IC triangle as the last symbol to be detected. Next, the symbols that overlap with the weakest user's symbol are added to the IC triangle. Then, all the symbols that overlaps the second weakest users' symbols are included to the IC triangle. This procedure is repeated until the strongest users' symbols are entered to the IC triangle. Once such an IC triangle is constructed for  $n$  number of transmissions

received from  $k_1$  to  $k_n$  users, the first symbol of the strongest user,  $k_1$ , is decoded. Next the consecutive symbols of  $k_1$  are decoded. Afterwards, the first symbol of the second strongest user,  $k_2$  is decoded by subtraction of prior estimated symbols of  $k_1$ . Then, the second symbol of the  $k_2$  user is decoded by subtracting the prior estimated symbols belonging to  $k_1$  and  $k_2$ . Next, the first symbol of  $k_3$  user is decoded by subtracting all the prior estimated symbols that belong to both  $k_1, k_2$  from the received signal  $Y$ . Similarly, the rest of the symbols of  $k_3$ , up to  $k_n$  users are decoded by subtracting the prior symbols estimated.

Moreover, the conventional T-SIC [17] is repeated iteratively between users for a fixed number of times,  $N_{\text{T-SIC}}$ . Specifically, the conventional T-SIC not only utilizes strong user signals to decode weak user signals but also uses weak user signals to decode strong user signals iteratively. In the Conv T-SIC scheme [17], the  $N_{\text{T-SIC}}$  is within the range  $1 \leq N_{\text{T-SIC}} \leq N_{\text{T-SICmax}}$ , where it is used primarily to improve the T-SIC accuracy in terms of BER. Furthermore, Conv T-SIC may not be optimal for decoders, particularly in massive D2D communication networks with energy-limited nodes. In the forthcoming section, a Cyclic T-SIC decoding scheme is proposed for A-NOMA to improve its decoding efficiency in terms of factors such as energy consumption, reliability, complexity, and delay is proposed.

#### B. CYCLIC T-SIC DECODING SCHEME

A Cyclic T-SIC scheme is proposed for A-NOMA D2D decoders comprising of three stages as, i) Optimization, ii) Decoding, and iii) Re-transmission.

##### 1) OPTIMIZATION STAGE

Let a superimposed signal is received at the receiver terminal  $R_X$ . Furthermore, to conserve the decoder energy consumption and reliability parameters, a binary optimization method is used by  $R_X$  as follows,

$$\text{maximize}_{D_{u_k}} \sum_{k=1}^K D_{u_k} (K - k + 1) \quad (7a)$$

$$\text{subject to } D_{u_k} \in \{0, 1\}, \forall k \in K \quad (7b)$$

$$D_{u_{(k+1)}} - D_{u_k} \leq 0 \quad (7c)$$

$$D_{u_k} (B \log_2(1 + \sum_{s=1}^{K-k+1} \gamma_k[s]) - R_{\min}) \geq 0 \quad (7d)$$

$$0 \leq \sum_{k^*=1}^K D_{u_{k^*}} \sum_{i \neq k^*}^K \sum_{\zeta=s-1}^{s+1} P_i g_i \Delta_{k^*,i}[s, \zeta] \leq I_{th}, \quad (7e)$$

where a decision vector of the data symbols to be decoded is introduced as  $\mathbf{D}_u = [D_{u_k}]_{k \in K}$ , and  $D_{u_k} = 1$  if the data symbols of the  $k$ th user are selected to be decoded. Further, the duration of symbol time that  $i$ th user overlap with the desired  $k^*$ th user symbol, co-channel interference threshold, and channel bandwidth are given by  $\Delta_{k^*,i}, I_{th}, B$  respectively. The

transmission power of  $k$ th user, channel gain of  $k$ th user, thermal noise variance, transmission power of  $i$ th user, channel gain of  $i$ th user are given by  $P_k, g_k, \sigma^2, P_i, g_i$ , respectively. Also,  $R_{min}$  is the minimum rate threshold defined for the communication system.

Moreover, the main aim of the optimization is to maximize the number of decoded data symbols while minimizing the energy consumption over computing, and hence an objective function is formulated using **Lemma 1**.

*Proposition 1:*  $D_{u_k}$  is approximated to a binary,  $D_{u_k} \in \{0, 1\}$ , by using a difference of two convex functions/sets constraint ( $D_b$ ) as follows [38]:

$$D_b = \{(D_{u_k} - D_{u_k}^2) \leq 0, \text{ if } 0 \leq D_{u_k} \leq 1\},$$

*Proof:* It is observed that,

$$(D_{u_k} - D_{u_k}^2) \in \{0, 1\}, \tag{8}$$

for any  $D_{u_k}$  satisfying  $0 \leq D_{u_k} \leq 1$ . It is noted that,  $(D_{u_k} - D_{u_k}^2) > 0$  when  $D_{u_k} \in (0, 1)$ . Thus satisfies  $(D_{u_k} - D_{u_k}^2) \leq 0$ , which is a convex inequality, only when  $D_{u_k} = 0$  or  $D_{u_k} = 1$ .  $\square$

*Lemma 1:* The number of symbols selected from an IC triangle per each  $k$ th user,  $N_{sym_k}$ , is given as,

$$N_{sym_k} = D_{u_k}(K - k + 1). \tag{9}$$

*Proof:* It is observed that the total number of symbols that is included in an IC triangle is  $K!$ . Further, the maximum number of symbols that overlap a symbol is two, since each data symbol is received over an equal  $T_{sym}$ . Hence, the total number of symbols starting from the weakest symbol increments from 1 to  $K$  for each  $k$ th user. Thus, for each  $k$ th user the number of symbols is  $(K - k + 1)$ , where  $k = 1$  denotes the strongest user. Moreover, the total number of users' data decoded,  $k_{opt} = \sum_{k=1}^K D_{u_k}$ .  $\square$

Moreover, the constraint in (7d) corresponds to the minimum rate, and (11f) corresponds to the maximum allowable co-channel interference constraint. Note that the optimization algorithm in (7a) involves non-linear constraints, such that the optimization is a hard constrained problem. Hence, it is reformulated by relaxing its binary variables and non-convex constraints. Additionally, the binary constraint in (7b) is transformed to linear constraints as given in (11b) and (11c). Such constraint re-formulation assure that  $D_{u_k}$  is approximated to a binary [39] using **Proposition 1**. Further, the non-linear constraint with regard to minimum rate constraint in (7d) is converted into a linear constraint as in (10), where  $\tilde{\gamma} = 2^{\frac{R_{min}}{B}} - 1$  [40].

$$D_{u_k}(\sigma^2 + \sum_{i=1}^K \sum_{\varsigma=s-1}^{s+1} P_i g_i \Delta_{k,i}[s, \varsigma] - P_k g_k (1 + \frac{1}{\tilde{\gamma}})) \leq 0. \tag{10}$$

The relaxed binary optimization with reformulated convex constraints is given as,

$$\text{maximize}_{D_{u_k}} \sum_{k=1}^K D_{u_k}(K - k + 1) \tag{11a}$$

$$\text{subject to } 0 \leq D_{u_k} \leq 1, \quad \forall k \in K \tag{11b}$$

$$\sum_{k=1}^K (D_{u_k} - D_{u_k}^2) \leq 0 \tag{11c}$$

$$D_{u_{(k+1)}} - D_{u_k} \leq 0 \tag{11d}$$

$$D_{u_k}(\sigma^2 + \sum_{i=1}^K \sum_{\varsigma=s-1}^{s+1} P_i g_i \Delta_{k,i}[s, \varsigma] - P_k g_k (1 + \frac{1}{\tilde{\gamma}})) \leq 0 \tag{11e}$$

$$0 \leq \sum_{k^*=1}^K D_{u_k} \sum_{i \neq k^*}^K \sum_{\varsigma=s-1}^{s+1} P_i g_i \Delta_{k^*,i}[s, \varsigma] \leq I_{th}, \tag{11f}$$

Moreover, the reformulated convex optimization problem in (11a) is solved efficiently by applying the Lagrangian dual algorithm using **Proposition 2**.

*Proposition 2:* The Lagrangian optimization problem is formed as,

$$\text{minimize}_{\lambda, \delta, \phi, \mu} \max_{D_u} \mathcal{L}(D_u, \lambda, \delta, \phi, \mu) \tag{12a}$$

$$\text{subject to } \lambda, \delta, \phi, \mu \succeq 0. \tag{12b}$$

where  $\lambda, \delta, \phi, \mu$  are the Lagrangian multipliers corresponding respectively to constraints in the optimization problem in (11a).

*Proof:* The Lagrangian objective function of problem in (11a) is formed as,

$$\begin{aligned} \mathcal{L}(D_u, \lambda, \delta, \phi, \mu) &= \sum_{k=1}^K D_{u_k}(K - k + 1) \\ &\quad - \sum_{k=1}^K \lambda_k D_{u_k} + \sum_{k=1}^K \lambda_k D_{u_k}^2 \\ &\quad - \sum_{k=1}^K \delta_k (D_{u_{(k+1)}} - D_{u_k}) \\ &\quad - \sum_{k=1}^K \phi_k \left( D_{u_k}(\sigma^2 + \sum_{i=1}^K \sum_{\varsigma=s-1}^{s+1} P_i g_i \Delta_{k,i}[s, \varsigma] - P_k g_k (1 + \frac{1}{\tilde{\gamma}})) \right) \\ &\quad - \left( \sum_{k^*=1}^K \mu_k D_{u_k} \sum_{i \neq k^*}^K \sum_{\varsigma=s-1}^{s+1} P_i g_i \Delta_{k^*,i}[s, \varsigma] - I_{th} \right), \end{aligned} \tag{13}$$

$\square$

Note that the objective function as well as all the constraints of the dual problem are linear with respect to the Lagrangian multipliers. Thus, the dual problem is convex over the dual variables  $\mu, \varsigma$  which can be optimized through one dimensional searching algorithm. Thus, the optimal  $D_u$

can be achieved by running a gradient descent algorithm [41]. First the gradient of the Lagrangian function with respect to  $D_{u_k}$  which is formulated as follows.

$$\nabla_{D_{u_k}} \mathcal{L} = -(K - k + 1) - \lambda_k + 2\lambda_k D_{u_k}. \quad (14)$$

Further,  $D_{u_k}$  can be updated as follows,

$$D_{u_k}^{(n)} = D_{u_k}^{(n-1)} + \beta \cdot \nabla_{D_{u_k}^{(n-1)}} \mathcal{L}, \quad (15)$$

where  $\beta$  denotes the iteration step size of  $D_{u_k}$ . After finding the optimal  $D_{u_k}$  using the gradient descent algorithm, the optimal  $\lambda$  can be achieved. Moreover, the dual function in (12a) is not guaranteed to be differentiable. Hence, an iterative scheme based on gradient descent algorithm is used to obtain the optimal  $\lambda, \delta, \phi, \mu$  [3] using **Proposition 3**.

*Proposition 3: The sub-gradient of the dual function,  $g(\lambda, \delta, \phi, \mu) = \max_{D_{u_k}} \mathcal{L}(D_{u_k}, \lambda, \delta, \phi, \mu)$ , with respect to  $\lambda, \delta, \phi, \mu$  can be derived as,*

$$\nabla_{\lambda} g(\lambda, \delta, \phi, \mu) = \sum_{k=1}^K D_{u_k} + \sum_{k=1}^K D_{u_k}^2, \quad (16)$$

$$\nabla_{\delta} g(\lambda, \delta, \phi, \mu) = D_{u_{(k+1)}} - D_{u_k}, \quad (17)$$

$$\nabla_{\phi} g(\lambda, \delta, \phi, \mu) = \sum_{k=1}^K \left( D_{u_k} \left( \sigma^2 + \sum_{i=1}^K \sum_{\varsigma=s-1}^{s+1} P_i g_i \Delta_{k,i}[s, \varsigma] - P_k g_k \left( 1 + \frac{1}{\gamma} \right) \right) \right), \quad (18)$$

$$\nabla_{\mu} g(\lambda, \delta, \phi, \mu) = \sum_{k^*=1}^K D_{u_k} \sum_{i \neq k^*}^K \sum_{\varsigma=s-1}^{s+1} P_i g_i \Delta_{k^*,i}[s, \varsigma] - I_{th}. \quad (19)$$

Further, the dual variable  $\lambda, \delta, \phi, \mu$  can be updated according to the following expression.

$$\lambda_k^{(m)} = \lambda_k^{(m-1)} + \alpha^{(m-1)} \nabla_{\lambda_k^{(m-1)}} \mathcal{L}, \quad \forall k \in K, \quad (20)$$

$$\delta_k^{(m)} = \delta_k^{(m-1)} + \alpha^{(m-1)} \nabla_{\delta_k^{(m-1)}} \mathcal{L}, \quad \forall k \in K, \quad (21)$$

$$\phi_k^{(m)} = \phi_k^{(m-1)} + \alpha^{(m-1)} \nabla_{\phi_k^{(m-1)}} \mathcal{L}, \quad \forall k \in K, \quad (22)$$

$$\mu_k^{(m)} = \mu_k^{(m-1)} + \alpha^{(m-1)} \nabla_{\mu_k^{(m-1)}} \mathcal{L}, \quad \forall k \in K, \quad (23)$$

where  $\alpha$  denotes the iteration step size of  $\lambda, \delta, \phi, \mu$ . The approach to solve the optimization problem in (7a) is summarized in Algorithm 1.

## 2) DECODING AND RE-TRANSMISSION STAGES

Once the optimal set of data symbols is derived using the proposed optimization in (11a), they are decoded using the Conv T-SIC scheme. Next, the  $R_X$  terminal repeats the process of listening to the same subcarrier and receiving retransmissions from the remaining users. Note that for outband D2D emergency scenarios, user signal retransmissions are necessary in order not to lose any critical data [42]. In addition, it is assumed that the network users follow a D2D protocol such as M-HELP [43], which is used for D2D emergency call transmissions. A M-HELP enabled UE re-transmits their own

### Algorithm 1 Optimization of T-SIC Triangle

---

**Data:**  $\gamma_k, \Delta_i$  of each  $k$ th user  
**Result:** Optimal  $D_{u_k}$

- 1 Initialize  $m = 0, \lambda^{(0)}, \delta^{(0)}, \phi^{(0)}, \mu^{(0)} \succcurlyeq 0$
- 2 Set error tolerances for algorithm termination,  $\epsilon_1, \epsilon_2$
- 3 **repeat**
- 4     Let  $p = 1$ ; Initialize  $D_{u_1}^{(0)}, D_{u_2}^{(0)}, D_{u_3}^{(0)}, \dots, D_{u_K}^{(0)}$
- 5     **repeat**
- 6         Run optimization problem in (11a)
- 7     **until**  $D_{u_k}$  converged, i.e.  $\|\nabla_{D_{u_k}^{(p-1)}} \mathcal{L}\|^2 \leq \epsilon_1$ ;
- 8     **for**  $k = 1:K$
- 9         Update  $D_{u_k}^{(p)}$  as in (15)
- 10     **end**
- 11      $p = p + 1$
- 12     Update  $\lambda^{(m)}, \delta^{(m)}, \phi^{(m)}, \mu^{(m)}$  as in (16), (17), (18), (23)
- 13      $m = m + 1$
- 14 **until**  $\lambda, \delta, \phi, \mu$  converged, i.e.,  $\|\lambda^{m-1} - \lambda^m\|^2 \leq \epsilon_2,$   
 $\|\delta^{m-1} - \delta^m\|^2 \leq \epsilon_2, \|\phi^{m-1} - \phi^m\|^2 \leq \epsilon_2,$   
 $\|\mu^{m-1} - \mu^m\|^2 \leq \epsilon_2$ ;
- 15 **Return**  $D_{u_k}$

---

data after a fixed time interval, when their data have not been forwarded up-to a pre-defined limit,  $n_{RS}$ , by neighbor devices. Here, the  $n_{RS}$  is calculated by transmitting users, which correspond to the number of relaying of its own data by the neighborhood. The re-transmitted data signals by transmitters share the same subcarrier and are superimposed such that it can be decoded using the optimization problem in (11a) at the  $R_X$  terminal. Correspondingly, this method is repeated until all  $K$  user data are decoded using the proposed optimization-assisted T-SIC.

To sum up, the procedure followed at the transmitting UEs is given in Algorithm 2, where  $n_{Rt}$  gives the data signal re-transmissions count.. Further, the Cyclic T-SIC scheme performed at the  $R_X$  terminal is summarized in Algorithm 3. Moreover, the method of decoding each user data using the proposed Cyclic T-SIC scheme is presented in Figure 2. First, a superimposed signal comprising  $K$  user data is received over a  $T_0$  duration. Optimization problem in (11a) is utilized to derive the optimal data symbol combination which comprises an IC triangle. Such data symbols are decoded using the T-SIC decoding scheme. In this case, received data symbols of some users can be left undecoded. Hence, after a  $T_0$  duration, retransmissions from such users occur after a  $t_r$  time interval and received as superimposed signals. The decoding procedure in Cyclic T-SIC is repeated for such a signal received. This procedure is repeated for an arbitrary  $r$  number of iterations until the successful decoding of each user data. Note that retransmissions from users are not mandatory in scenarios where all the user data are decoded in one Cyclic T-SIC iteration. Furthermore, the performance analysis of such a D2D A-NOMA decoding scheme in terms of energy efficiency, reliability, computational complexity, and delay aspects has been understudied.

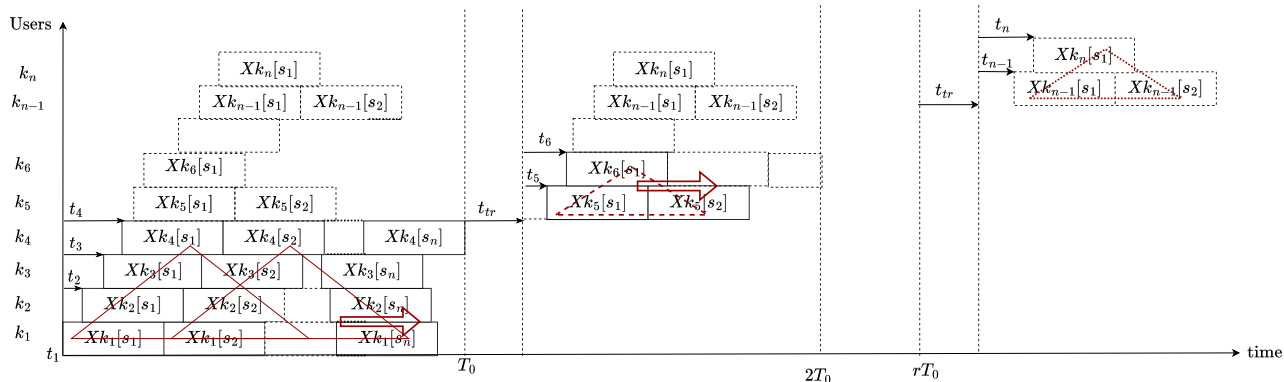


FIGURE 2. Proposed Cyclic T-SIC decoding scheme.

**Algorithm 2** At the Transmitter

- Data:** Relaying threshold ( $RS_{threshold}$ ), Retransmissions threshold, ( $n_{rth}$ )
- 1 Initialize  $n_{RS} = 0, n_{RT} = 0$
  - 2 **repeat**
  - 3     Listen to dedicated D2D emergency call channel
  - 4     Re-transmitting in the same resource in next period
  - 5 **until**  $n_{RS} \geq RS_{threshold}$  or  $n_{RT} \geq n_{rth}$ ;

**Algorithm 3** At the Receiver: Cyclic T-SIC Decoding

- Data:** Total number of users,  $K$ , sharing same resource
- 1 Initialize  $k_{opt} = 0$
  - 2 **repeat**
  - 3     Receive  $n(\leq K)$  user data superimposed signal
  - 4     Derive the optimal  $D_u$  using (11a)
  - 5     Decoding the  $k_{opt}(\leq n)$  user data
  - 6 **until** All  $K$  user data decoded;

**IV. PERFORMANCE ANALYSIS**

In this section the EE, average BER, computational complexity, and simulation delay of the proposed Cyclic T-SIC method are investigated.

**A. EE ANALYSIS**

The EE of the A-NOMA D2D scheme can be defined as the ratio between the total achievable rates and total power consumption of the communication system [3]:

$$EE = \frac{\sum_{k=1}^K B \cdot \log_2(1 + \gamma_k)}{\frac{1}{n_{sym} * T_{sym}} E_c + P_{circuit} + \varepsilon \sum_{k=1}^K P_k} \quad (24)$$

where  $E_c$  is the total energy consumption per SIC decoding cycle as defined in Lemma 2,  $P_{circuit}$  presents the power dissipated by user device hardware circuits [3], [40], and  $\varepsilon$  denotes the reciprocal of the transmitter power amplifier drain efficiency.

*Lemma 2: The total energy consumption per decoding instance is denoted by,*

$$E_c = E_{t-1} - E_t = E_{t-1} - E_{max} e^{-\frac{\log_e \frac{E_{initial}}{E_{final}}}{n_{sym2} N_{T-SIC1} - n_{sym1} N_{T-SIC2}} N_{T-SIC} \sum_{k=1}^K N_{sym_k(t)}}, \quad (25)$$

where  $E_{max}$  is the initial maximum energy in a user device,  $N_{T-SIC}$  is the number of repetitive times the same data symbols are decoded,  $n_{sym1}$  is the number of symbols decoded at the initial decoding and  $E_{initial}$  is the remaining energy after such decoding instance. Moreover, the total number of symbols decoded at  $t$  is  $n_{sym}(t) = \sum_{k=1}^K N_{sym_k}(t)$ . Also,  $E_{t-1}$ ,  $E_t$  are the residual energy levels in the  $(t - 1)$ th and  $t$ th instances. Further,  $n_{sym2}$  is the maximum number of symbols possible to decode with  $E_{max}$ , and  $E_{final}$  is the remaining energy at the end of decoding such  $n_{sym2}$ . Further, the behavior of such energy dissipation is illustrated in Figure 3.

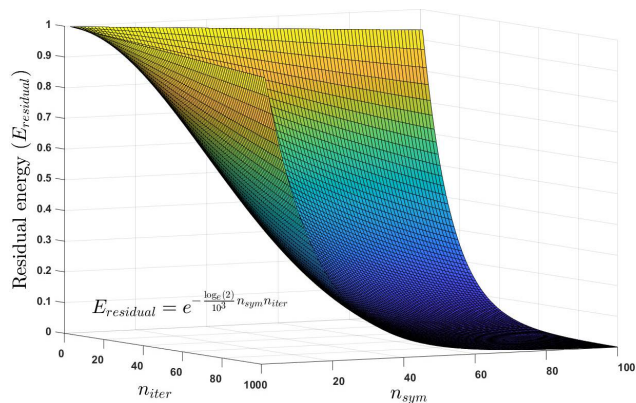


FIGURE 3. Residual energy of a user device in decoding  $n_{sym}$  number of symbols under  $N_{T-SIC}$ .

*Proof:* The energy consumption for decoding has an exponential deterioration depending on the  $n_{sym}$  [44]. The remaining energy after the initial decoding

instance is given as,

$$E_{\text{initial}} = E_{\text{max}} e^{-\alpha N_{\text{T-SIC}_1} n_{\text{sym}_1}}, \quad (26)$$

where  $\alpha$  denote the attenuation of energy depending on the receiver physical properties and processing efficiency. Moreover, the final remaining energy at the end of decoding  $n_{\text{sym}_2}$  is,

$$E_{\text{final}} = E_{\text{max}} e^{-\alpha N_{\text{T-SIC}_2} n_{\text{sym}_2}}. \quad (27)$$

From (26) and (27),

$$\alpha = \frac{\log_e \frac{E_{\text{initial}}}{E_{\text{final}}}}{n_{\text{sym}_2} N_{\text{T-SIC}_1} - n_{\text{sym}_1} N_{\text{T-SIC}_2}}. \quad (28)$$

□

Hence, the energy consumption per T-SIC decoding cycle for a specific  $\sum_{k=1}^K N_{\text{Sym}_k}$  and  $n_{\text{iter}}$  is formulated as,

$$\begin{aligned} E_c &= E_{t-1} - E_t, \\ &= E_{t-1} - E_{\text{max}} e^{-\frac{\log_e \frac{E_{\text{initial}}}{E_{\text{final}}}}{n_{\text{sym}_2} N_{\text{T-SIC}_1} - n_{\text{sym}_1} N_{\text{T-SIC}_2}} N_{\text{T-SIC}} \sum_{k=1}^K N_{\text{Sym}_k(t)}}. \end{aligned} \quad (29)$$

### B. BER ANALYSIS

The average theoretical BER of  $k^*$ th user data,  $P_{\text{bit},k^*}$ , in asynchronous transmissions can be formulated in [17] were updated as follows. First, by considering the latest detected symbols, the Signal to Interference Noise Ratio (SINR) of the  $s$ th symbol of the  $k^*$ th user is expressed with respect to  $\tilde{\eta}_{k^*}[s]$  as [17],

$$(\gamma_{k^*}[s]|z, h_{k^*}, \Delta_{k^*}) = \frac{P_{k^*} g_{k^*}}{\text{Var}(\tilde{\eta}_{k^*}[s]|z, h_{k^*}, \Delta_{k^*}) + \sigma^2}, \quad (30)$$

$$\gamma_{k^*}[s] = \frac{P_{k^*} g_{k^*}}{\text{Var}(\tilde{\eta}_{k^*}[s]|z, h_{k^*}, \Delta_{k^*}) + \sigma^2}, \quad (31)$$

where  $\mathbf{z}$  represents the latest detection status of the interfering symbols, i.e. correct or erroneous. Further, the error probability of  $s$ th symbol detection can be presented with respect to the  $(\tilde{\gamma}_k[s]|z, h_{k^*}, \Delta_{k^*}[s])$  as [17],

$$\begin{aligned} P(e_{k^*}[s]|z, h_{k^*}, \Delta_{k^*}[s]) \\ = 1 - \left( 1 - Q \left( \sqrt{\frac{3 \cdot (\tilde{\gamma}_k[s]|z, h_{k^*}, \Delta_{k^*}[s])}{2 \cdot (M-1)}} \right) \right)^2, \end{aligned}$$

where,  $Q(\cdot)$  represent the Q function and  $M$  denotes the order in  $M$ -QAM [45].

$$(\tilde{\gamma}_k[s]|z, h_{k^*}, \Delta_{k^*}[s]) = \text{Var}(\tilde{\eta}_k[s]|z, \Delta_{k^*}[s]) + \sigma^2 > d_{e_k^*} \quad (32)$$

where  $d_{e_k^*}$  is half the distance between two nearest constellation points given by  $\sqrt{\frac{3 \cdot P_{k^*} h_{k^*}}{2 \cdot (M-1)}}$  [46]. Further, the conditional error probability of the  $s$ th symbol detection can

be obtained as [17],

$$\begin{aligned} P(e_{k^*}[s]|h_{k^*}, \Delta_{k^*}[s]) \\ = \sum_{i=1}^{2^{(k_{\text{opt}}-1)}} P(e_{k^*}[s]|iP_{z(\mathcal{L})}, h_{k^*}, \Delta_{k^*}[s]) \\ \cdot \prod_{k \in k_{\text{opt}}, \zeta \in (s-1, s+1), k \neq k^*} Pr_{i,k}^{(\mathcal{L})}[\zeta], \end{aligned}$$

where,

$$\begin{aligned} P(e_{k^*}[s]) &= \frac{1}{\tau_{\text{max}} - \tau_{\text{min}}} \\ &\cdot \int_{\tau_{\text{min}}}^{\tau_{\text{max}}} \int_0^{\infty} P(e_{k^*}[s]|h_{k^*}, \Delta_{k^*}[s]) \\ &\cdot e^{-h_{k^*}} \cdot dh_{k^*} \cdot d\Delta_{k^*}[s], \end{aligned} \quad (33)$$

$$P_{\text{bit},k^*} = \frac{P(e_{k^*}[s])}{\log_2(M)}, \quad (34)$$

where  $P(e_{k^*}[s])$ ,  $P(e_{k^*}[s]|\alpha_{k^*}, \Delta_{k^*}[s])$  denote respectively, the probability of error and conditional probability of error on the  $s$ th symbol of the  $k^*$ th user. Also,  $s$ th symbol of the  $k^*$  user is the desired symbol to be detected and  $M$  is the modulation order. Further,  $h_{k^*}$  denotes the magnitude of fading for the  $s$ th symbol of the  $k^*$ th user. The  $\Delta_{k^*}[s]$  denotes the percentage of symbol time that the overlapping symbols of the  $i$ th user has on the  $s$ th symbol of the  $k^*$ th user. Moreover,  $iP_{z(\mathcal{L})}$ , denotes probability of the  $i$ th permutation of  $\mathbf{z}$ ,  $1 \leq i \leq 2^{(k_{\text{opt}}-1)}$  and  $Pr_{i,k}[\zeta]$  denotes the probability of detection being correct or in error.

### C. COMPUTATIONAL COMPLEXITY ANALYSIS

The computational complexity of decoding  $K$  user data under Conv T-SIC and Cyclic T-SIC are presented as follows.

- 1) Conv T-SIC: The total interference to the desired symbol  $s$ th symbol of  $k^*$ th user,  $\eta_{k^*}[s]$ , is successively cancelled in Conv T-SIC process and hence the maximum computational complexity depends on the number of user devices,  $K$ , which is approximately of order  $O(K^2)$  [3].
- 2) Cyclic T-SIC: The decoding process of the proposed method has a complexity of  $O(k_{\text{opt}}^2)$ , where  $k_{\text{opt}} \leq K$ . On top of that, the computational complexity for the stochastic gradient descent method based optimization in the Cyclic T-SIC scheme is in the order of  $O(\log(\frac{1}{\epsilon}))$  [3]. To sum up, the proposed Cyclic T-SIC method has a computational complexity of  $O(\log(\frac{1}{\epsilon})k_{\text{opt}}^2)$  per single decoding iteration. Further, it is proven from **Lemma 3** that the computational complexity in Cyclic T-SIC scheme is lower than the Conv T-SIC scheme.

*Lemma 3: The computational complexity of Cyclic T-SIC decoding of  $k_i$  users' data over  $n$  iterations is less than that of Conventional SIC decoding of  $K$  users' data in one iteration [3]. Note that  $k_i$  corresponds to  $k_{\text{opt}}$  in the  $i^{\text{th}}$  iteration and the sum of  $k_i$  equals  $K$ .*

$$\log \left( \frac{1}{\epsilon} \right) \sum_{i=1}^n k_i^2 \leq K^2, \quad (35)$$

where,  $0.1 < \epsilon < 1$ ,  $k_i \leq K$  and  $\sum_{i=1}^n k_i = K$ .

*Proof:* Consider

$$K = k_1 + k_2 + k_3 + \dots + k_i + \dots + k_{n-1} + k_n, \quad (36)$$

where  $k_i \leq K$ . Hence,

$$k_i^2 \leq K^2. \quad (37)$$

Further, it can be seen that,

$$\sum_{i=1}^n k_i^2 \leq \left( \sum_{i=1}^n k_i \right)^2, \quad (38a)$$

$$\sum_{i=1}^n k_i^2 \leq K^2. \quad (38b)$$

Moreover,

$$\log \left( \frac{1}{\epsilon} \right) \sum_{i=1}^n k_i^2 < K^2, \quad (39)$$

where  $0.1 \leq \epsilon < 1$ . □

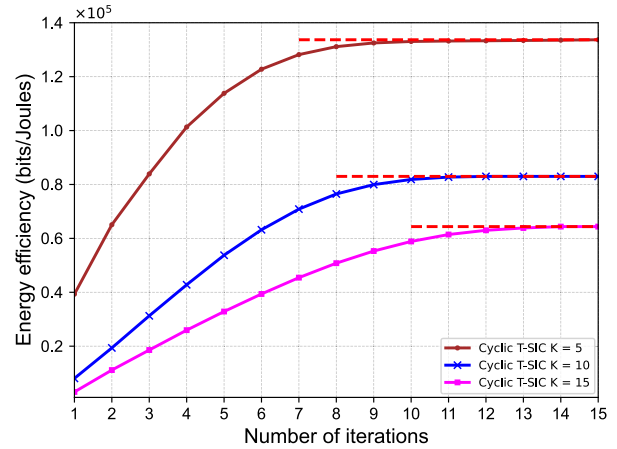
### V. ANALYSIS OF THE NUMERICAL SIMULATION RESULTS

In this Section, the numerical simulation results are presented to demonstrate the performance of the proposed system model and the algorithm. User terminals are considered to be randomly located within a radius of 100m to the corresponding receiving UE. Also, for a Monte-Carlo simulation analysis,  $10^3$  random A-NOMA D2D setups are considered. Different parameters used for simulation analysis are summarized in TABLE 1.<sup>2</sup> Furthermore, the performance of both the Conv T-SIC and Cyclic T-SIC are considered under the condition that each IC triangle formed across the received asynchronous NOMA signal is decoded for one iteration, i.e.,  $N_{T-SIC} = 1$ .

TABLE 1. Simulation parameters.

Parameter	Value
Modulation order, $M$	16 QAM
Minimum relative symbol time offset, $\tau_{min}$	0.01 sec
Maximum relative symbol time offset, $\tau_{max}$	0.5 sec
Maximum initial energy of user device, $E_{max}$	1.08 kJ
Power dissipated by user device, $P_{circuit}$	0.01 W
Maximum transmit power, $P_{max}$ [47]	0.2 W (23 dBm)
Path-loss exponent, $\eta$	1.5
Minimum throughput threshold, $R_{min}$	2 Mbits/sec
Interference threshold, ( $I_{th}$ )	1.2W
Number of repeated times of T-SIC decoding, $N_{T-SIC}$	1
AWGN power, $\sigma^2$	0.01 W
Bandwidth, $B$	1 MHz
Symbol time duration, $T_{sym}$	1 sec
Error tolerance for optimal $D_u$ , $\epsilon_1$	0.1
Error tolerance for optimal $\lambda$ , $\epsilon_2$	0.5
Learning rates, $\alpha$ and $\beta$	0.4
Transmission power of an UE	[0, ..., $P_{max}$ ]
Total number of UEs, $K$	[2, ..., 25]
Relative symbol time offset, $\phi$	[1 - 50]% $T_{sym}$
Received power ratio, $\nu$	[1, ..., 10]
Transmit SNR	[10, ..., 35] dBm

<sup>2</sup>It is noteworthy that these given values can be modified to any other values depending on the specific scenario under consideration.



\* K values were selected arbitrarily. However it is a variable and can be adjusted suitably.

FIGURE 4. Convergence of EE under the optimization algorithm in the Cyclic T-SIC scheme against the number of iterations. Parameters:  $\nu = 5$ ,  $I_{th} = 1.2 W$ ,  $\phi = 50\%$ .

Figure 4 depicts that the Energy Efficiency (EE) obtained via the proposed optimization algorithm converges to a stable value within a fixed number of iterations. However, the converging EE value decreases as the  $K$  increases. With the increment in the  $K$ , the total  $n_{sym}$  to be decoded increases, which considerably elevates  $E_c$  and reduces the EE. Furthermore, the number of iterations required to converge EE increases with the increment in  $K$ . This is mainly due to the fact that the vector size of  $D_u$  increments with  $K$ .

FIGURE 5 depicts the EE performance versus  $K$  with Cyclic and Conv T-SIC under different  $I_{th}$  values. It can be seen from the plot that EE decreases when the value  $K$  increases. The total  $n_{sym}$  symbols increment with  $K$  and hence result in a higher  $E_c$ . Moreover, when the  $I_{th}$  increases,  $n_{sym}$  increases and reduces the EE. It is also noteworthy that since Conv T-SIC is not optimizing the  $K$ , it is not impacted by  $I_{th}$ . Furthermore, in Conv T-SIC, the total  $K$  data are decoded during one decoding iteration which leads to a higher number of computations and thereby a higher  $E_c$  compared to Cyclic T-SIC. It is noteworthy that in Figure. 4 and Figure. 5, Cyclic T-SIC, EE converges respectively under  $K = 5$ ,  $K = 10$  and  $K = 15$ , to  $1.3 \times 10^5$ ,  $8.3 \times 10^4$  and  $6.4 \times 10^4$  bits per Joule at  $I_{th} = 1.2 W$ . Similarly, under Conv T-SIC, EE converges respectively under  $K = 5$ ,  $K = 10$  and  $K = 15$ , to  $7 \times 10^4$ ,  $3.6 \times 10^4$  and  $2 \times 10^4$  bits per Joule at  $I_{th} = 1.2 W$ .

Figure 6 depicts the variation of EE against the received power ratio,  $\nu$ . It is seen from the plot that the EE increases as  $\nu$  increments in both Cyclic and Conv T-SIC schemes.  $P_k$  increases with the elevation of  $\nu$ , which leads to the increment in  $\gamma_k$  and the average sum throughput, which improves the EE. Moreover, Cyclic T-SIC has a significant improvement in comparison to Conv T-SIC, because the increment in  $\nu$  enables the optimization algorithm to derive  $D_u$  easily due to the distinct  $P_k$  levels of each user. Hence, the  $D_u$  derivation enables the optimal data symbols to be decoded. Also, a convergence in EE in the Cyclic T-SIC is observed when

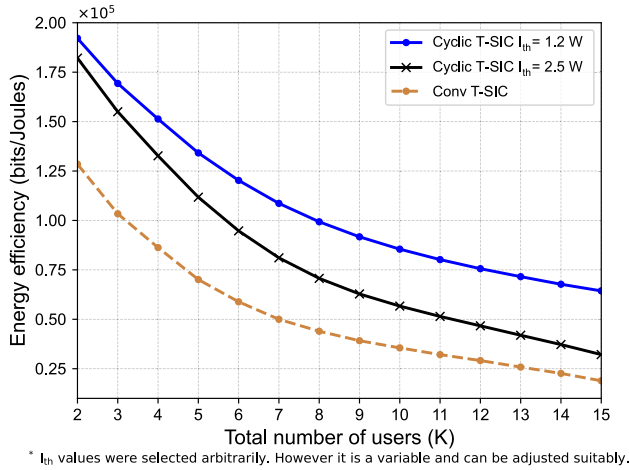


FIGURE 5. EE vs total number of users under varying interference threshold constraints. Parameters:  $\nu = 5$ ,  $\phi = 50\%$ .

$\nu \geq 5.0$ . This is due to the thresholds in the optimization algorithm which limits the  $k_{opt}$  decoded per iteration.

Furthermore, it can be seen from the Figure. 5 and Figure. 6 that Cyclic T-SIC, EE converges respectively under  $K = 5, K = 10$  and  $K = 15$ , to  $1.3 \times 10^5, 8.3 \times 10^4$  and  $6.4 \times 10^4$  bits per Joule at  $\nu = 5$ . Similarly, under Conv T-SIC, EE converges respectively under  $K = 5, K = 10$  and  $K = 15$ , to  $7 \times 10^4, 3.6 \times 10^4$  and  $2 \times 10^4$  bits per Joule at  $\nu = 5$ . In this scenario, the Cyclic T-SIC has relative EE gains by 52.5%, 32.8%, and 38.1% compared to Conv T-SIC under  $K = 5, K = 10$ , and  $K = 15$ .

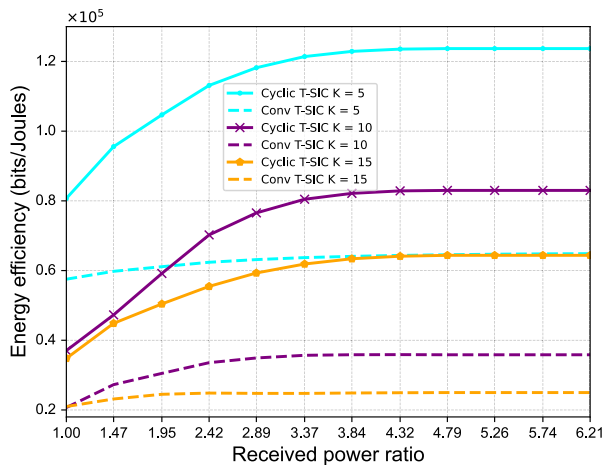


FIGURE 6. Energy efficiency vs received power ratio ( $\nu$ ) under varying number of users. Parameters:  $I_{th} = 1.2 \text{ W}$ ,  $\phi = 50\%$ .

FIGURE 7 illustrates the variation of EE against  $K$  under different  $\nu$  values. Further, with the elevation in  $\nu$ s, an increment in EE of the Cyclic T-SIC is observed because  $D_u$  is derived optimally considering the significant gaps between each  $k$  users in terms of  $\gamma_k$ .

Further, it can be observed that consistent results are obtained in Figure. 6 and Figure. 7. In Cyclic T-SIC, EE converges respectively under  $\nu = 1, \nu = 2$  and  $\nu = 5$ , to  $4 \times 10^5, 6 \times 10^4$  and  $8.3 \times 10^4$  bits per Joule at  $K = 10$ . Similarly, under Conv T-SIC, EE converges respectively under  $\nu = 1, \nu = 2$  and  $\nu = 5$ , to  $2 \times 10^4, 3.2 \times 10^4$  and  $3.6 \times 10^4$  bits per Joule at  $K = 10$ .

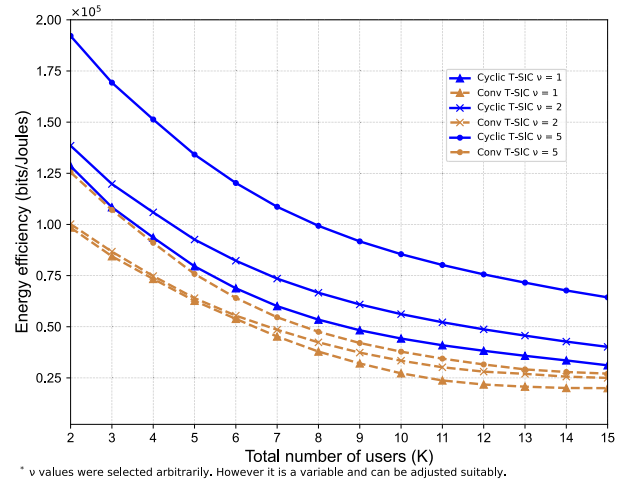
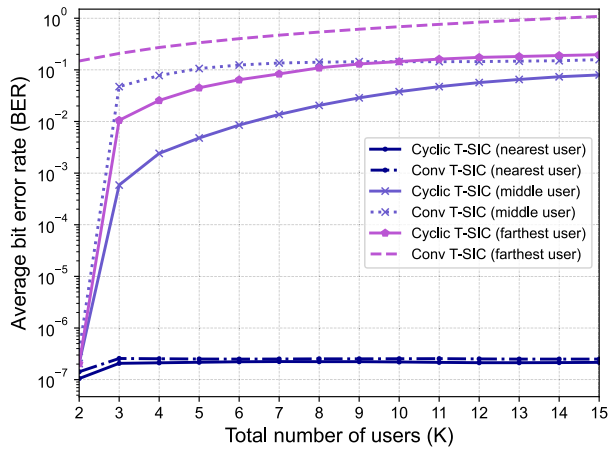


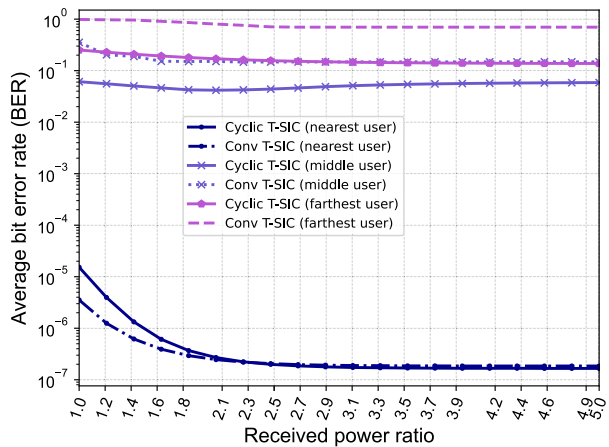
FIGURE 7. Energy efficiency vs total number of users. Parameters:  $I_{th} = 1.2 \text{ W}$ ,  $\phi = 50 \%$ , transmit SNR = 23 dBm.

Figure 8a depicts the average BER against  $K$  under Cyclic T-SIC and Conv T-SIC. The BER of both schemes increment against  $K$  since with a higher  $K$ , the  $\gamma_k$  difference among user data decreases. This lowers the accuracy of the received data detection, which impacts the decoding process. Moreover, the average BER in Cyclic T-SIC is lower than Conv T-SIC. The main reason behind this is that the Cyclic T-SIC scheme derives the optimal  $k_{opt}$  to decode based on the  $D_u$  derived. The availability of distinct  $\gamma_k$  values between the user data decoded in the Cyclic T-SIC scheme increases the accuracy in decoding. Further, the Cyclic T-SIC decodes all  $K$  data over successive iterations by taking into consideration of the  $\gamma_k$  of each user data. Conversely, Conv T-SIC decodes such data in a single iteration, which increases the BER.

Figure 8b depicts the BER against the  $\nu$  for the nearest user, middle user, and farthest user. A significant BER gap is seen between the nearest user and middle user. As  $\nu$  increases, a comparable  $\gamma_k$  level difference is seen between the near user and far user. Hence, the decoding accuracy reduces as the  $\gamma_k$  gap increases between consecutive users. The highest  $\gamma_k$  level is received from the nearest user. Under  $\nu < 2$ , the Cyclic T-SIC has a higher BER than Conv T-SIC. The reason being that when  $\nu < 2$ , the interference faced by the nearest user is higher than the estimated interference using Cyclic T-SIC. In the proposed optimal  $D_u$  of Cyclic T-SIC, only a set of selected users are decoded assuming that the interference from the remaining users is minimum. Hence, the decoding error is higher than Conv T-SIC. Meanwhile, as  $\nu \gtrsim 2$ , the interference from the remaining users on the near user



(a) BER vs number of users ( $K$ ).

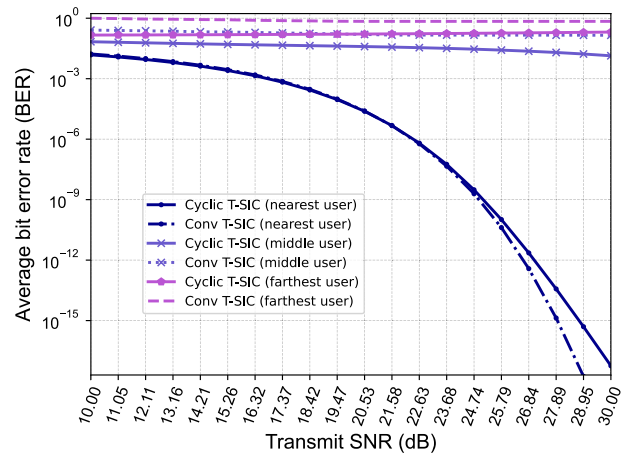


(b) BER vs received power ratio ( $\nu$ ).

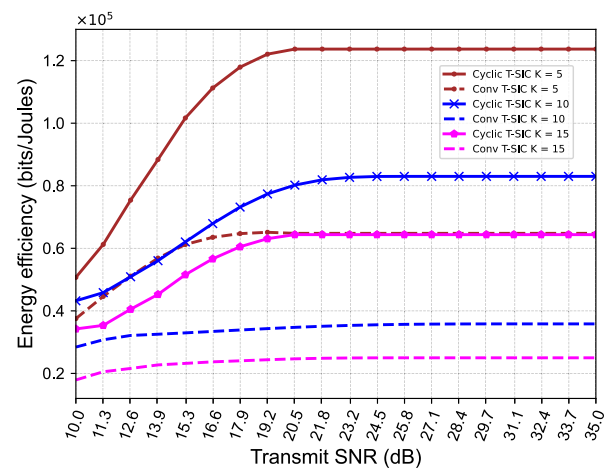
**FIGURE 8.** BER analysis of nearest, middle, and farthest users under Cyclic and Conv T-SIC schemes. Parameters:  $\nu = 2$ ,  $I_{th} = 1.2$  W, transmit SNR = 23 dBm,  $\phi = 50\%$ ,  $K = 10$ .

is less significant and hence the decoding accuracy is high and similar to Conv T-SIC. Furthermore, for the middle and farthest users' BER of Cyclic T-SIC is lesser compared to Conv T-SIC. In the middle and farthest user case, the  $\gamma_k$  of the consecutive users is minimum that Cyclic T-SIC decodes the user data during a successive iteration of Cyclic decoding utilizing the retransmissions from the transmitters. Thereby, the  $\gamma_k$  level of the received signals from the middle and farthest users are sufficiently high enough during the successive iteration since the stronger signals also do not interfere.

Figure 9a depicts the BER performance against the transmit SNR under the Cyclic T-SIC and Conv T-SIC schemes. BER in Cyclic T-SIC is lower than Conv T-SIC for the case where transmit SNR is  $< 23$  dBm. The optimal  $D_u$  derivation depending on the  $\gamma_k$  levels of each  $k$ th user and  $I_{th}$  constraint increases the accuracy of decoding. Meanwhile when the transmit SNR  $\approx 23$  dBm, BER of Cyclic T-SIC  $>$  BER of Conv T-SIC. The difference between  $\gamma_k$  levels of each  $k$ th user is less significant when all users transmit at SNR  $\approx 23$  dBm. Hence, The optimal  $D_u$  derivation is less accurate, thereby increasing the BER in Cyclic T-SIC.



(a) BER vs transmit SNR for  $\nu = 2$ .

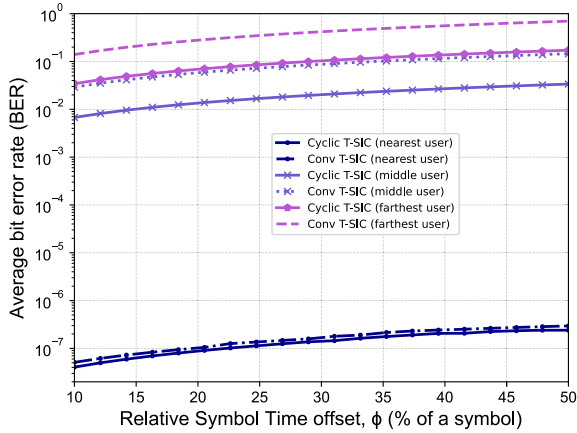


(b) EE vs transmit SNR for  $\nu = 5$ .

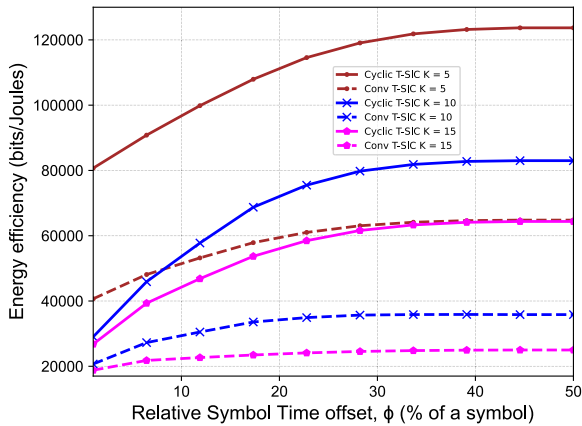
**FIGURE 9.** BER and EE analysis of the proposed Cyclic T-SIC. Parameters:  $I_{th} = 1.2$  W,  $\phi = 50\%$ ,  $K = 10$ .

Moreover, Figure 9b depicts that the EE of the proposed system is higher than Conv T-SIC, because the optimal  $D_u$  reduces the  $E_c$  per decoding iteration. Moreover, with a lower transmit SNR, a higher EE can be gained using Cyclic T-SIC compared to the Conv T-SIC scheme. Jointly considering the results obtained in Figure 7 and Figure 9b, following insights can be drawn. In Cyclic T-SIC, EE converges respectively under  $K = 5, K = 10$  and  $K = 15$ , to  $1.3 \times 10^5, 8.3 \times 10^4$  and  $6.4 \times 10^4$  bits per Joule at transmit SNR = 23 dBm. Similarly, under Conv T-SIC, EE converges respectively under  $K = 5, K = 10$  and  $K = 15$ , to  $7 \times 10^4, 3.6 \times 10^4$  and  $2 \times 10^4$  bits per Joule at transmit SNR = 23 dBm.

Figure 10a represents the BER performance against the relative symbol time offset,  $\phi$ , between users under Cyclic and Conv T-SIC schemes. The BER performance worsens with the increment in  $\phi$  since the co-channel interference increases. However, the Cyclic T-SIC has a reduced BER because of deriving the optimal  $D_u$  to select  $n_{sym}$  decoded per iteration based on the  $I_{th}$ . Figure 10b, depicts that the EE of Cyclic T-SIC is higher than Conv T-SIC, although the



(a) BER vs relative symbol time offset ( $\phi$ ) for  $\nu = 2$ .



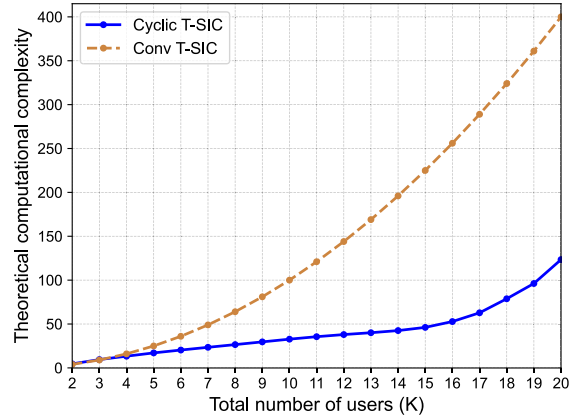
(b) EE vs relative time offset ( $\phi$ ) for  $\nu = 5$ .

**FIGURE 10. BER and EE analysis of the proposed Cyclic T-SIC against relative symbol time offset. Parameters:  $I_{th} = 1.2$  W,  $\nu = 5$ , transmit SNR = 23 dBm,  $K = 10$ .**

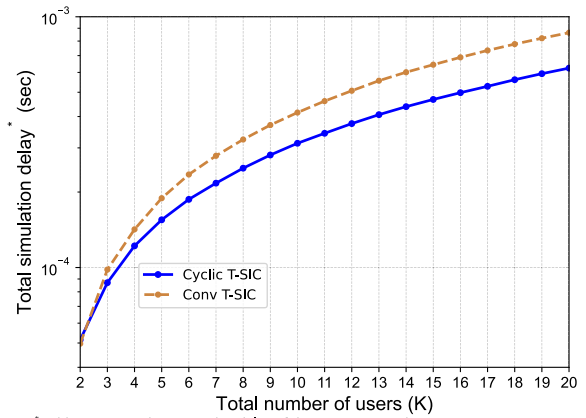
co-channel interference between users increased with the  $\phi$ . The optimization of number of user data decoded based on the  $I_{th}$  limits the  $k_{opt}$  decoded per iteration. This results in reducing the interference among the symbols which are decoded and improves the EE of Cyclic T-SIC compared to Conv T-SIC. Further, it is observed that a lower BER and higher EE can be obtained using the Cyclic T-SIC scheme, even if the  $\phi$  increases the asynchrony among the received data signals. In addition, EE starts converging after the  $\phi \gtrsim 0.3$ . BER converges since  $I_{th}$  and minimum rate thresholds are reached with the  $K = 10$  and hence the same  $D_u$  is obtained, and the  $n_{sym}$  reaches a maximum limit.

In Cyclic T-SIC, EE converges respectively under  $K = 5, K = 10$  and  $K = 15$ , to  $1.3 \times 10^5, 8.3 \times 10^4$  and  $6.4 \times 10^4$  bits per Joule at transmit SNR = 23 dBm and  $\phi = 50\%$ , proving the consistency between results obtained in Figure. 9b and Figure. 10b. Similarly, under Conv T-SIC, EE converges respectively under  $K = 5, K = 10$  and  $K = 15$ , to  $7 \times 10^4, 3.6 \times 10^4$  and  $2 \times 10^4$  bits per Joule at transmit SNR = 23 dBm and  $\phi = 50\%$ .

Figure. 10b depicts the BER performance of nearest, middle, and farthest users against  $\phi$ . In general, the BER performance worsens with the increment in  $\phi$  since the co-channel



(a) Computational complexity vs total number of users ( $K$ ). Parameters: interference threshold ( $I_{th}$ ) = 1.2 W, received power ratio,  $\nu = 5, \phi = 50\%$ .



\* With respect to the processing delay of the computer used

(b) Total simulation delay vs total number of users ( $K$ ). Parameters: interference threshold ( $I_{th}$ ) = 1.2 W, received power ratio,  $\nu = 5, \phi = 50\%$ .

**FIGURE 11. Computational complexity and simulation delay of proposed Cyclic T-SIC.**

interference increases. The BER of the nearest user of both Cyclic and Conv T-SIC schemes are nearly similar since, the nearest user data has a significant  $\gamma_k$  level in both schemes which increases the accuracy of decoding its data. Moreover, the Cyclic T-SIC of both middle and farthest users have significantly reduced BER compared to Conv T-SIC because of decoding their data in successive iterations of Cyclic T-SIC with the use of retransmissions. This leads to deriving the optimal  $D_u$  and selecting  $n_{sym}$  decoded per iteration based on the  $I_{th}$ .

Moreover, consistent results are obtained in Figure. 8a, Figure. 8b, Figure. 9a and Figure. 10a under  $K = 10, \nu = 2$ , transmit SNR = 23 dBm and  $\phi = 50\%$ . The BER value of respectively the nearest user, middle user, and farthest user converges to approximately  $2.2 \times 10^{-7}, 0.037$  and  $0.14$  under Cyclic T-SIC. The BER value of respectively the nearest user, middle user, and farthest user converges approximately to  $2.2 \times 10^{-7}, 0.15$  and  $0.68$  under Conv T-SIC.

Figure 11a depicts the theoretical computational complexity against  $K$  under Cyclic and Conv T-SIC schemes.

The curve with the Cyclic T-SIC has a considerably lower complexity compared to the Conv T-SIC. In Cyclic T-SIC, the user data are decoded in sequential iterations, where only  $k_{opt} \leq K$  data is decoded per iteration. In contrast, Conv T-SIC decodes the total  $K$  data in a single iteration. Hence, a complexity reduction of 56.14% by Cyclic T-SIC over Conv T-SIC is observed in this case.

The Figure 11b depicts the total simulation delay against  $K$  under Cyclic T-SIC and the Conv T-SIC schemes. The average simulation delay in Cyclic T-SIC is lower than that of Conv T-SIC. As  $K$  increases, the decoding delay increases in Conv T-SIC decoding. In contrast, the delay is less in Cyclic T-SIC since  $k_{opt} \leq K$  per decoding iteration. The delay decreases with the successive iterations as the  $k_{opt}$  data decoded in such iterations decreases. Also, the Cyclic T-SIC achieves a simulation delay reduction of 22.44% compared to Conv T-SIC in this case. Note that the complexity reduction of the proposed scheme is in Figure. 11a is significantly higher than the simulation delay in Figure. 11b. Complexity analysis is done under theoretical assumptions and in contrast simulation delay is measured with respect to the processing delay of the computer used. Hence, depending on the processing speed and other hardware delays, the corresponding decoding delay of the proposed scheme is varying as in Figure. 11b.

## VI. CONCLUSION

In this paper, we have designed a Cyclic T-SIC scheme to reduce decoding complexity, energy consumption, and bit error rate of a superimposed signal received in a massive A-NOMA enabled D2D network. The proposed scheme's performance was verified through a computer-based Monte-Carlo simulation analysis. The Cyclic T-SIC showed a significant EE improvement in comparison to Conv T-SIC. The optimization algorithm in Cyclic T-SIC enabled the receiver terminal to derive the optimal symbols to decode under to the co-channel interference and data rate constraints. Further, it was observed that Cyclic T-SIC achieves a lower BER and higher EE due to the optimization algorithm, even if the asynchrony among the received data signals is  $\phi \approx 0.3$ . Furthermore, a convergence in EE and BER in the Cyclic T-SIC was observed when  $\nu \geq 5.0$  and the transmit SNR  $\geq 23$  dBm due to the thresholds in the optimization algorithm which limits the  $k_{opt}$  decoded per iteration. Also, the decoding complexity and delay were less in Cyclic T-SIC since  $k_{opt} \leq K$  per decoding iteration. As a future direction, investigating the performance of the proposed scheme for 5G Ultra-Reliable Low Latency Communications (URLLC) is an interesting extension to this work.

## REFERENCES

[1] V. Basnayake, D. N. K. Jayakody, V. Sharma, N. Sharma, P. Muthuchidambaramanathan, and H. Mabed, "A new green prospective of non-orthogonal multiple access (NOMA) for 5G," *Information*, vol. 11, no. 2, p. 89, Feb. 2020. [Online]. Available: <https://www.mdpi.com/2078-2489/11/2/89>

[2] H. Baek, W. J. Yun, S. Jung, J. Park, M. Ji, J. Kim, and M. Bennis, "Communication and energy efficient slimmable federated learning via superposition coding and successive decoding," 2021, *arXiv:2112.03267*.

[3] J. Tang, J. Luo, M. Liu, D. K. C. So, E. Alsusa, G. Chen, K.-K. Wong, and J. A. Chambers, "Energy efficiency optimization for NOMA with SWIPT," *IEEE J. Sel. Topics Signal Process.*, vol. 13, no. 3, pp. 452–466, Jun. 2019.

[4] M. Agiwal, H. Kwon, S. Park, and H. Jin, "A survey on 4G-5G dual connectivity: Road to 5G implementation," *IEEE Access*, vol. 9, pp. 16193–16210, 2021.

[5] H. I. Fitriarsari, A. I. Lestari, D. L. Luhurkinanti, and R. F. Sari, "Performance evaluation of downlink multi-user OFDMA scheduling in 5G new radio (NR)," in *Proc. 18th Int. Conf. Electr. Eng./Electron., Comput., Telecommun. Inf. Technol. (ECTI-CON)*, May 2021, pp. 219–223.

[6] T. D. Kumar and P. Venkatesan, "Performance estimation of multicarrier CDMA using adaptive brain storm optimization for 5G communication system in frequency selective fading channel," *Trans. Emerging Telecommun. Technol.*, vol. 31, p. e3829, 2020, doi: [10.1002/ett.3829](https://doi.org/10.1002/ett.3829).

[7] J. Zhao, Y. Liu, K. K. Chai, Y. Chen, M. Elkashlan, and J. Alonso-Zarate, "NOMA-based D2D communications: Towards 5G," in *Proc. IEEE Global Commun. Conf. (GLOBECOM)*, Dec. 2016, pp. 1–6.

[8] Y. Liu, W. Yi, Z. Ding, X. Liu, O. A. Dobre, and N. Al-Dhahir, "Developing noma to next generation multiple access (NOMA): Future vision and research opportunities," *IEEE Wireless Commun.*, vol. 29, no. 6, pp. 1–8, Dec. 2022.

[9] Z. Ding, R. Schober, and H. V. Poor, "Unveiling the importance of SIC in NOMA systems—Part 1: State of the art and recent findings," *IEEE Commun. Lett.*, vol. 24, no. 11, pp. 2373–2377, Nov. 2020.

[10] F. M. Caceres, S. Kandeepan, and S. Sun, "Theoretical analysis of hybrid SIC success probability under Rayleigh channel for uplink CR-NOMA," *IEEE Trans. Veh. Technol.*, vol. 71, no. 10, pp. 1–16, Oct. 2022.

[11] X. Wang, F. Labeau, and L. Mei, "Asynchronous uplink non-orthogonal multiple access (NOMA) with cyclic prefix," in *Proc. IEEE Wireless Commun. Netw. Conf. (WCNC)*, Apr. 2018, pp. 1–6.

[12] M. Ganji, X. Zou, and H. Jafarkhani, "Asynchronous transmission for multiple access channels: Rate-region analysis and system design for uplink NOMA," *IEEE Trans. Wireless Commun.*, vol. 20, no. 7, pp. 4364–4378, Jul. 2021.

[13] X. Li, H. Liu, G. Li, Y. Liu, M. Zeng, and Z. Ding, "Effective capacity analysis of AmBC-NOMA communication systems," *IEEE Trans. Veh. Technol.*, vol. 71, no. 10, pp. 1–6, Oct. 2022.

[14] W. Chen and Z. Tang, "Research on improved receiver of NOMA-OFDM signal based on deep learning," in *Proc. Int. Conf. Commun., Inf. Syst. Comput. Eng. (CISCE)*, May 2021, pp. 173–177.

[15] S. Gamboa, F. J. Cintron, D. Griffith, and R. Rouil, "Adaptive synchronization reference selection for out-of-coverage proximity services," in *Proc. IEEE 28th Annu. Int. Symp. Pers., Indoor, Mobile Radio Commun. (PIMRC)*, Oct. 2017, pp. 1–7.

[16] C. Liu and N. C. Beaulieu, "Exact BER performance for symbol-asynchronous two-user non-orthogonal multiple access," *IEEE Commun. Lett.*, vol. 25, no. 3, pp. 764–768, Mar. 2021.

[17] H. Hacı, H. Zhu, and J. Wang, "Performance of non-orthogonal multiple access with a novel asynchronous interference cancellation technique," *IEEE Trans. Commun.*, vol. 65, no. 3, pp. 1319–1335, Mar. 2017.

[18] F. Lu, M. Xu, L. Cheng, J. Wang, and G.-K. Chang, "Power-division non-orthogonal multiple access (NOMA) in flexible optical access with synchronized downlink/asynchronous uplink," *J. Lightw. Technol.*, vol. 35, no. 19, pp. 4145–4152, Oct. 1, 2017.

[19] X. Zou, B. He, and H. Jafarkhani, "An analysis of two-user uplink asynchronous non-orthogonal multiple access systems," *IEEE Trans. Wireless Commun.*, vol. 18, no. 2, pp. 1404–1418, Feb. 2019.

[20] X. Zou, B. He, and H. Jafarkhani, "On uplink asynchronous non-orthogonal multiple access systems with timing error," in *Proc. IEEE Int. Conf. Commun. (ICC)*, May 2018, pp. 1–6.

[21] J. Liu, Y. Li, G. Song, and Y. Sun, "Detection and analysis of symbol-asynchronous uplink NOMA with equal transmission power," *IEEE Wireless Commun. Lett.*, vol. 8, no. 4, pp. 1069–1072, Aug. 2019.

[22] X. Zou, M. Ganji, and H. Jafarkhani, "Cooperative asynchronous non-orthogonal multiple access with power minimization under QoS constraints," *IEEE Trans. Wireless Commun.*, vol. 19, no. 3, pp. 1503–1518, Mar. 2020.

- [23] W. U. Khan, M. A. Javed, T. Nguyen, S. Khan, and B. ElHalawany, "Energy-efficient resource allocation for 6G backscatter-enabled NOMA IoV networks," *IEEE Trans. Intell. Transp. Syst.*, vol. 23, no. 7, pp. 1–11, Jul. 2021.
- [24] V. Basnayake, H. Mabed, D. N. K. Jayakody, P. Canalda, and M. Beko, "Adaptive emergency call service for disaster management," *J. Sensor Actuator Netw.*, vol. 11, no. 4, p. 83, Nov. 2022. [Online]. Available: <https://www.mdpi.com/2224-2708/11/4/83>
- [25] V. Basnayake, H. Mabed, P. Canalda, and D. N. K. Jayakody, "Enhanced convex hull based clustering for high population density avoidance under D2D enabled network," in *Proc. IEEE 94th Veh. Technol. Conf. (VTC-Fall)*, Sep. 2021, pp. 1–7.
- [26] U. S. S. S. Arachchilage, D. N. K. Jayakody, S. K. Biswash, and R. Dinis, "Recent advances and future research challenges in non-orthogonal multiple access for 5G networks," in *Proc. IEEE 87th Veh. Technol. Conf. (VTC Spring)*, Jun. 2018, pp. 1–6.
- [27] R. Shankar, "Examination of a non-orthogonal multiple access scheme for next generation wireless networks," *J. Defense Model. Simul., Appl., Methodology, Technol.*, vol. 19, no. 3, pp. 453–465, Jul. 2022.
- [28] A. Zafar, M. Shaqfeh, M.-S. Alouini, and H. Alnuweiri, "On multiple users scheduling using superposition coding over Rayleigh fading channels," *IEEE Commun. Lett.*, vol. 17, no. 4, pp. 733–736, Apr. 2013.
- [29] X. Chen, L. Pu, L. Gao, W. Wu, and D. Wu, "Exploiting massive D2D collaboration for energy-efficient mobile edge computing," *IEEE Wireless Commun.*, vol. 24, no. 4, pp. 64–71, Aug. 2017.
- [30] S. Qureshi, S. A. Hassan, and D. N. K. Jayakody, "Successive bandwidth division NOMA systems: Uplink power allocation with proportional fairness," in *Proc. 14th IEEE Annu. Consum. Commun. Netw. Conf. (CCNC)*, Jan. 2017, pp. 998–1003.
- [31] S. Rajkumar and D. N. K. Jayakody, "Backscatter assisted NOMA-PLNC based wireless networks," *Sensors*, vol. 21, no. 22, p. 7589, Nov. 2021.
- [32] I. Raziah, Y. Yunida, Y. Away, R. Muharrar, and N. Nasaruddin, "Adaptive relay selection based on channel gain and link distance for cooperative out-band device-to-device networks," *Heliyon*, vol. 7, no. 7, Jul. 2021, Art. no. e07430. [Online]. Available: <https://www.sciencedirect.com/science/article/pii/S2405844021015334>
- [33] S. Kumarapandian and M. J. Sibley, "Complexity analysis of double-threshold based relay selection in d2d cooperative network," *J. Wireless Netw. Commun.*, vol. 8, no. 1, pp. 1–6, 2018.
- [34] P. S. Bithas, K. Maliatsos, and F. Foukalas, "An SINR-aware joint mode selection, scheduling, and resource allocation scheme for D2D communications," *IEEE Trans. Veh. Technol.*, vol. 68, no. 5, pp. 4949–4963, May 2019.
- [35] O. Hayat, R. Ngah, S. Z. Hashim, M. H. Dahri, R. F. Malik, and Y. Rahayu, "Device discovery in D2D communication: A survey," *IEEE Access*, vol. 7, pp. 131114–131134, 2019.
- [36] M. Koivisto, M. Costa, J. Werner, K. Heiska, J. Talvitie, K. Leppänen, V. Koivunen, and M. Valkama, "Joint device positioning and clock synchronization in 5G ultra-dense networks," *IEEE Trans. Wireless Commun.*, vol. 16, no. 5, pp. 2866–2881, May 2017.
- [37] A. A. Nasir, S. Durrani, H. Mehrpouyan, S. D. Blostein, and R. A. Kennedy, "Timing and carrier synchronization in wireless communication systems: A survey and classification of research in the last five years," 2015, *arXiv:1507.02032*.
- [38] E. Che, H. D. Tuan, and H. H. Nguyen, "Joint optimization of cooperative beamforming and relay assignment in multi-user wireless relay networks," *IEEE Trans. Wireless Commun.*, vol. 13, no. 10, pp. 5481–5495, Oct. 2014.
- [39] S. He, J. Yuan, Z. An, W. Huang, Y. Huang, and Y. Zhang, "Joint user scheduling and beamforming design for multiuser MISO downlink systems," 2021, *arXiv:2112.01738*.
- [40] E. Bjornson, M. Kountouris, and M. Debbah, "Massive MIMO and small cells: Improving energy efficiency by optimal soft-cell coordination," in *Proc. ICT*, May 2013, pp. 1–5.
- [41] X. Wang, L. Yan, and Q. Zhang, "Research on the application of gradient descent algorithm in machine learning," in *Proc. Int. Conf. Comput. Netw., Electron. Autom. (ICCNEA)*, Sep. 2021, pp. 11–15.
- [42] O. Gama, P. Carvalho, J. A. Afonso, and P. M. Mendes, "Trade-off analysis of a MAC protocol for wireless e-emergency systems," in *Systems and Software*, S. Hailes, S. Sicari, and G. Roussos, Eds. Berlin, Germany: Springer, 2010.
- [43] V. Basnayake, H. Mabed, D. N. K. Jayakody, and P. Canalda, "M-HELP—multi-hop emergency call protocol in 5G," in *Proc. IEEE 19th Int. Symp. Netw. Comput. Appl. (NCA)*, Nov. 2020, pp. 1–8.
- [44] J.-S. Ahn, J.-H. Yoon, and K.-W. Lee, "Performance and energy consumption analysis of 802.11 with FEC codes over wireless sensor networks," *J. Commun. Netw.*, vol. 9, no. 3, pp. 265–273, Sep. 2007.
- [45] S. M. Sadinov, "Simulation study of M-ARY QAM modulation techniques using MATLAB/Simulink," in *Proc. 40th Int. Conv. Inf. Commun. Technol., Electron. Microelectron. (MIPRO)*, May 2017, pp. 547–554.
- [46] A. Goldsmith, *Wireless Communications*. Cambridge, U.K.: Cambridge Univ. Press, 2005.
- [47] P. Joshi, F. Ghasemifard, D. Colombi, and C. Tornevik, "Actual output power levels of user equipment in 5G commercial networks and implications on realistic RF EMF exposure assessment," *IEEE Access*, vol. 8, pp. 204068–204075, 2020.



**VISHAKA BASNAYAKE** received the B.Sc. degree in electrical and electronic engineering from the University of Peradeniya, Sri Lanka, in 2017, and the M.Sc. degree in wireless communication engineering from the University of Oulu, Finland, in 2019. She is currently pursuing the Ph.D. degree with Université Bourgogne Franche Comte (UBFC), France, in collaboration with Sri Lanka Technological Campus (SLTC), Sri Lanka. Her research interests include D2D communication in cellular wireless networks, asynchronous NOMA, optimization, localization, network protocol design, and distributed learning.



**DUSHANTHA NALIN K. JAYAKODY** (Senior Member, IEEE) received the M.Sc. degree in electronics and communications engineering from the Department of Electrical and Electronics Engineering, Eastern Mediterranean University, Turkey, and the Ph.D. degree in electronics and communications engineering from University College Dublin, Ireland, in 2013. From 2014 to 2016, he was a Postdoctoral Research Fellow at the University of Tartu, Estonia, and the University of Bergen, Norway. Since 2021, he has been with the Autónoma TechLab, Portugal, and the Department of Engineering and Computer Science, Universidade Autónoma de Lisboa, Portugal. He has been working as the Head of the School of Postgraduate and Research, Sri Lanka Technological Campus (SLTC), Padukka, Sri Lanka; and the Founding Head of the Centre of Telecommunication Research, SLTC, since January 2019. He has published nearly 200 international peer-reviewed journals and conference papers and books. His research interests include PHY and NET layer prospective of 5G communications technologies, such as NOMA for 5G, cooperative wireless communications, device to device communications, LDPC codes, and unmanned aerial vehicle. He is a fellow of IET. He currently serves as an Area Editor for the *Physical Communications* journal (Elsevier), *Information journal (MDPI)*, *Sensors (MDPI)*, and *Internet Technology Letters (Wiley)*. He also serves on the Advisory Board for *Journal of Multidisciplinary Sciences (MDPI)*. In addition, he serves as a reviewer for various IEEE TRANSACTIONS and other journals.



**HAKIM MABED** received the M.S. degree from the University of Algiers, Algeria, in 2000, and the Ph.D. degree from the University of Angers, France, in 2003. He is currently an Associate Professor with the University of Bourgogne Franche-Comté (UBFC), France. He is part of the FEMTO-ST Institute (UMR CNRS 6174) and the Complex Networks Team, where he does his research. He led and participated to different funded research projects (SOES, ALGOPDF,

WIFIOPF) in collaboration with THALES, Orange Labs, and DGA. He has authored or coauthored more than 60 international publications. His research interests include distributed intelligent MEMS, wireless communications, combinatorial optimization, and programmable matter.



**AMBRISH KUMAR** received the M.Tech. degree in optical and wireless communication technologies from the Jaypee University of Information Technology, Solan, Himachal Pradesh, India, and the Ph.D. degree in wireless communication from the University of Delhi, Delhi, India. He was a Network Engineer at Tata Communication Pvt. Ltd., New Delhi, and a Lecturer at Amity University Rajasthan, Jaipur, India. He was a Teaching-cum Research Fellow (TRF) at the Netaji Subhas Uni-

versity of Technology (Formerly Netaji Subhas Institute of Technology (NSIT)), New Delhi. He was a Researcher at the Department of Information and Communications Engineering, Pukyong National University (PKNU), Busan, South Korea. He is currently a Postdoctoral Researcher with the Centre for Telecommunications Research (CTR), Sri Lanka Technological Campus, Padukka, Sri Lanka. His research interests include physical layer security, visible light communication, underwater VLC, ultraviolet communication, free-space-optics, and cognitive radio networks.



**THARINDU D. PONNIMBADUGE PERERA** (Member, IEEE) received the B.Sc. (Hons.) and M.Sc. degrees from the Department of Computing, Faculty of ACES, Sheffield Hallam University, U.K., and the Ph.D. degree in systems, networks and devices of telecommunications from the Highest Attestation Commission (VAK), Russia, and Tomsk Polytechnic University, in February 2015. He worked as a Research Engineer at the School of Computer Science and Robotics, National

Research Tomsk Polytechnic University. He is currently working as a Senior Lecturer and a Research Scientist with the Sri Lanka Technological Campus. His research interests include information and communication theory, RF-energy harvesting, interference exploitation, UAV communications, and channel coding. He has been awarded a full-time scholarship from the Ministry of Education, Russian Federation for Ph.D. studies.

...